SELF-DRIVING LABORATORIES FOR AUTONOMOUS DISCOVERY OF NEW MATERIALS

by
UTKARSH PRABHAKAR GUPTA

A thesis submitted to the ELECTRICAL AND COMPUTER ENGINEERING DEPARTMENT,
CULLEN COLLEGE OF ENGINEERING
in partial fulfillment of the requirements for the degree of

MASTER OF SCIENCE

in ELECTRICAL ENGINEERING

Chair of Committee: DR. XIAONAN SHAN

Committee Member: DR. JIEFU CHEN

Committee Member: DR. JIMING BAO

University of Houston
May 2025

Copyright 2025, Utkarsh Prabhakar Gupta

DEDICATION

To my parents, Prabhakar Gupta and Nitu Gupta, for your endless love, sacrifices, and unwavering belief in me. This journey would not have been possible without you.

ACKNOWLEDGMENTS

I would like to express my sincere gratitude to my supervisor, Dr. Xiaonan Shan, for their invaluable guidance, encouragement, and continuous support throughout the course of this research. Their insights and expertise greatly shaped the direction and quality of this work.

I am also thankful to my committee members, Dr. Jiefu Chen, Dr. Jiming Bao, for their thoughtful feedback and constructive suggestions that helped improve the quality of my thesis.

Special thanks to my research colleagues, Nandakishore Ravi, Xiliang Zhao and Gegari Mannariyath Thomas for the helpful discussions, collaboration, and shared enthusiasm during long hours in the lab.

I also extend my appreciation to the faculty and staff of the Electrical and Computer Engineering at University of Houston, whose assistance made this journey smoother.

ABSTRACT

Rapid discovery of efficient electrocatalysts is a cornerstone in the advancement of sustainable energy technologies such as water electrolysis. However, conventional trial-and-error experimental workflows are slow, labor-intensive, and poorly suited for exploring vast compositional spaces. This thesis presents the design and implementation of a fully automated, modular self-driving laboratory system capable of autonomously synthesizing and characterizing multi-metallic catalysts for the oxygen evolution reaction (OER) and hydrogen evolution reaction (HER).

The system integrates mechanical, electronic, and software components in a tightly orchestrated workflow. Python-controlled SCARA robotic arms perform all experimental steps—including precursor mixing, electrode loading, deposition, rinsing, and evaluation—without human intervention aside from periodic replacement of consumables like stock solutions and electrode substrates. Mechanically, the platform features a 3D-printed, custom-designed interchangeable working electrode holder for stainless steel mesh substrates, as well as modular reservoir stands. A single-layer PCB, etched and fabricated in-house, connects to 11 electrode holders to a CHI 660E single-channel potentiostat via magnetic contacts, enabling sequential electrochemical processing.

The electrochemical deposition and evaluation of binary and ternary catalysts—including NiFe, NiFeCo, and NiMoP systems—are conducted in 1 M KOH. Techniques such as cyclic voltammetry (CV), chronoamperometry/chronopotentiometry (CP), and

electrochemical impedance spectroscopy (EIS) are used to assess catalyst performance. Electrodes are automatically rinsed in deionized water between steps, and simple optical inspection is enabled via robotic positioning in front of a fixed zoom camera. Experimental data are collected and processed by a custom Python pipeline that performs iR correction, extracts relevant metrics (e.g., overpotential at 10 mA/cm^2 for OER, potential at 10 mA/cm^2 for HER, and resistance at zero phase from EIS), and generates comparative plots across compositional ratios. Ternary compositional maps are used to visualize performance trends and guide further testing.

Although all workflows are currently driven by user-defined parameters, the platform is designed for future integration with machine learning frameworks—such as Graph Neural Networks (GNNs) or Bayesian Optimization—to enable closed-loop, data-driven catalyst optimization. By combining autonomous robotics with scalable electrochemical analysis and modular hardware design, this work lays a robust foundation for accelerated discovery and screening of electrocatalysts using self-driving lab methodologies.

TABLE OF CONTENTS

Dedication iii

Acknowledgments iii

ABSTRACT iii

List of Figures iii

CHAPTER 1 Introduction 1

CHAPTER 2 System Architecture & Automation Workflow 6

2.1 Automated Experiment Sequence 6

2.2 Dispensing Solution Mixing Logic & Control 14

2.3 Reservoir Hardware 17

2.4 Liquid-Handling Hardware Evolution 19

CHAPTER 3 Hardware & Fixture Design 23

3.1 Electrode Holder Evolution 23

3.2 Printed-circuit backplane 25

3.3 Multi-Reservoir System with Swappable Electrode Bundles 26

3.4 Final Modular Electrode Holder Design 27

3.5 Transition to Working Electrode Optimization 28

CHAPTER 4 Working Electrode Design Optimization 29

4.1 Importance of Orientation and Positioning in Repeatability 29

4.2 First Modular Frame Design 31

4.3 Bubble Formation and Redesign 32

4.4 Final Integration with Electrode Holder 33

CHAPTER 5 Automated Data Analysis and Visualization 35

5.1 Pipeline Overview & Motivation 35

5.2 Processing Pipeline 35

5.3 Interpolation Methods for Ternary Mapping 36

5.4 Performance Metrics and Visualization 37

5.5 Example Output and Applications 37

5.6 Scalability and Reusability 38

CHAPTER 6 Catalyst Screening Results 39

6.1 Bimetallic Catalysts 39

6.1.1 NiFe Series 39

6.1.2 NiCu Series 40

6.2 Trimetallic Catalysts 41

6.2.1 NiFeCo 41

6.2.2 NiMoP 42

References 45

LIST OF FIGURES

Figure 1-1 Project Diagram. 5
Figure 2-1 Complete process overview diagram. 8
Figure 2-2 The core control thread of the autonomous system. 10
Figure 2-3 Individual tools that construct the autonomous system. 11
Figure 2-4 The entire autonomous catalyst screening system. a) Side view. b) Top view. 12
Figure 2-5 Parts of the complete process. a) Solution preparation. b) Electrode holder manipulation. c) Working electrode attachment d) Electrode washing. e) Sample imaging. f) Electrode detachment. 13
Figure 2-6. Automatic solution preparation process diagrams. a) Updated version with optimized sequence logic. b) Earlier version using a less efficient aspiration-dispense loop and linear reservoir traversal. 16
Figure 2-7 Stock solution reservoirs in the experimental setup. 18
Figure 2-8 Original solution dispensing setup. a) Linear stage with syringe. b) Syringe held on the end effector of the robot. 21
Figure 3-1 First version of electrode holder. 23
Figure 3-2 Electrode holder with magnetic pins. a) Singular setup. b) Multiple sets for large batch of experiments. 24
Figure 3-3 a) Initial prototype with magnets and long wires. b) 3D model of the PCB beneath the tube stand. 26
Figure 3-4 Electrode holder with magnetically attaching working electrode. 27
Figure 4-1 CV curves comparing two versions of working electrodes clips. a) Traditional design with stainless steel clips to attach mesh. b) Newest design with standardized orientation. 30
Figure 4-2 Working electrode clip designs. 31
Figure 4-3 Bubble formation problem. a) Bubble formation during OER. b) Uneven deposition on top of stainless steel mesh. 32
Figure 4-4 Improved design. a) Working electrode clip without the hinge mechanism. b) Deposition results using new design. 33
Figure 4-5 Working electrode clip with reinforced walls 33
Figure 6-1 NiFe results. a) CV scans with different NiFe ratios. b) Overpotential at 10 mA/cm^2 39
Figure 6-2 NiCu results. a) CV scans with different NiFe ratios. b) Overpotential at 10 mA/cm^2. 40
Figure 6-3 NiFeCo results. a) CV scans with different NiFeCo ratios. b) Ternary plot with overpotential at 10 mA/cm^2. c) Ternary plot with nearest neighbor interpolation. d) Ternary plot with radial basis function interpolation. 41
Figure 6-4 NiFeCo results from a different batch. 42
Figure 6-5 NiMoP HER results for overpotential at 10 mA/cm^2. a) Scatter plot. b) Plot with nearest neighbour interpolation. c) Plot with RBF interpolation. 43
Figure 6-6 NiMoP OER results. a) CV scans with different NiMoP ratios. b) Ternary plot with overpotential at 10 mA/cm^2. c) Ternary plot with nearest neighbor interpolation. 44

CHAPTER 1 INTRODUCTION

The progress of human society has always depended on discovering and developing new materials, which have greatly influenced fields like energy, healthcare, environmental protection, agriculture, and transportation[1–3]. From early tools made of iron to modern batteries powering electric cars, materials have driven technological breakthroughs that solve major global problems. However, traditional methods for finding new materials, often called the Edisonian approach, rely on trial-and-error testing. This involves making and checking many material combinations, which takes a lot of time, money, and effort because the range of possible chemicals and structures is huge. Even after finding a promising material, it often needs complex changes to work in real applications, slowing down the process further[4–6]. These old methods struggle to keep up with the need for fast innovation and can't fully tackle urgent issues like clean energy, pollution, or growing healthcare needs in a world with more people and fewer resources.

Catalysts are especially important because they speed up chemical reactions used in industries and environmental solutions, such as making fuels, reducing emissions, or producing medicines[7]. Finding and improving catalysts, though, is a major challenge in materials science. Traditional catalyst testing requires time-consuming steps—mixing chemicals, analysing results, and checking performance—often based on small tweaks or guesses rather than a clear plan. Designing a catalyst means balancing factors like how well it works, how specific it is, how long it lasts, and how much it

costs, all while matching the needs of a particular reaction. For example, creating catalysts for clean hydrogen production or turning carbon dioxide into useful products involves testing countless options, which is too much for old methods to handle efficiently. These slow processes not only delay discoveries but also make it hard to quickly meet new technological or societal demands, showing the need for better ways to find catalysts.

Recently, high-throughput experimentation (HTE) has become a useful way to speed up material and catalyst discovery. HTE allows researchers to test many material combinations at once, saving time and resources compared to traditional methods[8]. But HTE still depends on human decisions and set plans, which can miss unexpected possibilities or focus only on familiar materials. A newer approach, called self-driving laboratories (SDLs), takes this further by combining automation with smart computer methods. SDLs use robots, automated chemical mixing, real-time analysis tools (like spectroscopy that watches reactions as they happen), and machine learning (ML) programs to explore large sets of chemicals and materials on their own[9,10]. These systems work faster and more accurately than people, making decisions based on data to improve experiments step-by-step.

SDLs work by blending machines and smart software. Robots handle repetitive jobs, like preparing samples or collecting data, so researchers can focus on bigger ideas, like coming up with new questions or understanding results. ML programs look at experiment outcomes right away, spotting trends, suggesting better material mixes, and guiding the system to find the best catalysts with fewer tests. For example, ML can pick experiments that improve a catalyst's performance, cutting down the number of trials

needed. SDLs also use advanced tools to check reactions in real time, giving instant feedback to plan the next step. This continuous process is much faster than the stop-and-go nature of older methods, offering a smart and efficient way to discover new materials.

The benefits of SDLs go beyond just saving time. These systems make advanced research easier for smaller teams or labs with less funding, as they don't need as many people or expensive equipment. SDLs can also explore unusual materials that might be ignored in traditional labs because they take too long to test[9]. For instance, finding new catalysts for eco-friendly processes—like capturing carbon or recycling plastics—could happen faster with SDLs that test many options systematically. In a world facing problems like climate change or the need for affordable medicines, quickly developing better catalysts is vital. SDLs could help science move faster and create solutions that improve lives.

Still, building SDLs isn't easy. Creating a system that combines robots, sensors, data systems, and ML programs requires everything to work together smoothly, even when experiments change. Making sure automated tests are accurate and repeatable is another issue, as is designing ML programs that can handle the messy, complex data from materials research. Also, setting up an SDL can be costly at first, even if it saves money later. These challenges show why we need focused research to build reliable, affordable, and easy-to-use SDLs for specific tasks like catalyst testing.

This thesis aims to tackle these issues by designing an automatic lab for autonomous catalyst screening, creating a practical and efficient system for finding new materials. Based on SDL ideas, the lab will use automated chemical mixing, catalysts

deposition/synthesis, and real-time analysis to evaluate the catalyst performance, and make discovery of catalysts faster while using fewer resources. Unlike older high-throughput systems that test everything randomly, our system could use smart programs such as AI prediction model to focus on the best possibilities. By targeting catalyst screening—which is important for energy, environmental, and chemical industries—this project will show how autonomous labs can work well. The research will also look at real-world factors, like keeping costs low and making the system usable in different settings, to ensure it can be used outside the lab. This work matters because it could change how we find catalysts. An autonomous lab might shorten the time to develop new catalysts from years to months, helping solve problems faster—like making clean fuels or improving drug production. The ideas from this project could also apply to other areas, like batteries or nanotechnology, making them useful for more than just catalysts. Through this research, we hope to add to the growing field of autonomous labs, showing how automation and smart systems can lead to quicker, better discoveries in materials science.

In the chapters ahead, we first present the overall system architecture and automated workflow (Chapter 2). Within that chapter we also describe the solution-dispensing module that prepares precursor mixtures. Chapter 3 details the hardware fixtures—including the robotic electrode holder—and the procedures used for catalyst synthesis. Chapter 4 focuses on working-electrode optimisation, highlighting design iterations that improve repeatability. Chapter 5 explains our automated data-analysis pipeline, covering iR-correction, ternary mapping, and visualisation tools used to evaluate catalyst performance. Finally, Chapter 6 presents the screening results for

bimetallic (NiFe, NiCu) and trimetallic (NiFeCo, NiMoP) catalysts. By covering both the technical and scientific facets of a self-driving laboratory, this thesis offers a comprehensive guide to autonomous experimentation and demonstrates how such platforms accelerate materials discovery.

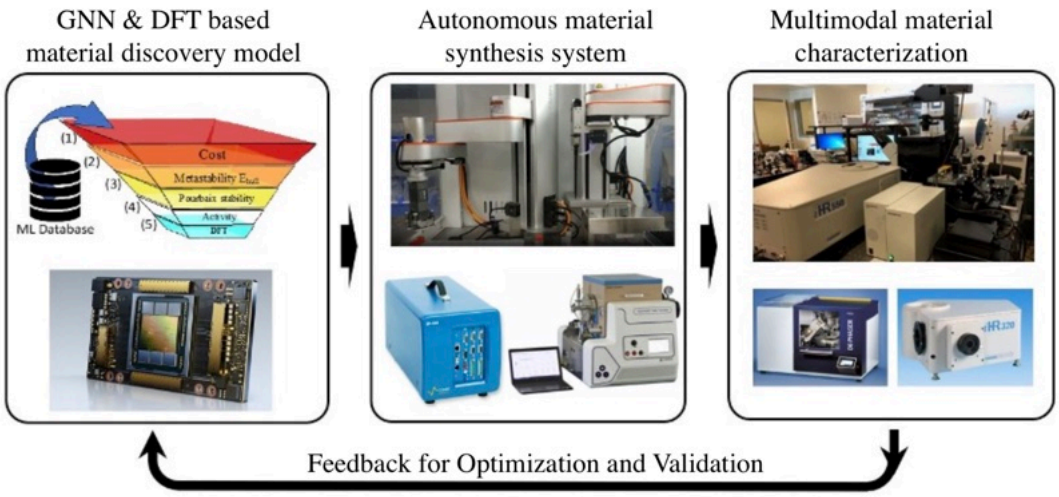

Figure 1-1 Project Diagram.

CHAPTER 2 SYSTEM ARCHITECTURE & AUTOMATION WORKFLOW

In this chapter, we introduce the architecture of our autonomous system, detailing its individual components and the procedure for material screening. Our autonomous system focuses on the electrochemical deposition of metal alloys for various applications. All the control is realized by python code. We will control: the robotic arms for solution mixing and electrode manipulations, potentiostat for electrochemical deposition and performance evaluation, and camera for electrode imaging;

2.1 Automated Experiment Sequence

1) "Experiment Planning". We start our system from the experimental planning step. In this stage, we will first enter how many metal compositions ('n') we are going to synthesize in this run, it could be 1, 2 ,3, 4 or even large number if needed. This will indicate how many stock solutions we are going to mix in each tube. Then we need to set up number of reservoirs ('m') for solution mixing and catalysts deposition. If we want to prepare 11 different combinations of solution and deposit the metal alloys/catalysts in these 11 different combinations, we need to input $m = 11$. Right now, we have 11 reservoirs, and we can prepare more than 11 samples at the same time. For example, we can screen for 22 catalysts/chemical combinations at once, since 22 is bigger than 11 (maximum number of tubes available for solution mixing and

deposition), we will run two batches of experiments (11 samples per batches) to match the goal.

2) “Solution mixing using Robot 1”. Our system uses Selective Compliance Assembly Robot Arm (SCARA) which allows us to manipulate the syringe pump and pipette tip for solution dispersion. We use a 3D printer to prepare large stock solutions containers. For example, when we are screening 3 different metal ions to form alloys, we will use three stock solution containers. The robotic arm will bring the syringe pump and the pipette tip into the first stock solution reservoir, suck in the solution, and distribute to different tubes (for example, 11 tubes). The amount of the solution for each tube will be automatically calculated using the python program we have made. After each individual solution dispensing, the pipette tip will be brought to a rinsing beaker and the tip will be rinsed totally to minimize the cross contamination.

3) “Robotic arm 2 for electrode manipulation and catalysts synthesis”. Following solution mixing, the second SCARA robotic arm handles electrode manipulation for catalyst deposition. We have designed a specialized electrode holder to secure the counter electrode (a platinum plate) and the reference electrode (Ag/AgCl) in fixed positions while establishing electrical connections to a three-pin pogo magnet connector. When the holder is placed into any tube for electrochemical deposition or performance evaluation, the pogo magnet connector automatically forms a reliable electrical contact via magnetic attraction. This enables precise control of the electrodes by the potentiostat, facilitating seamless electrochemical operations

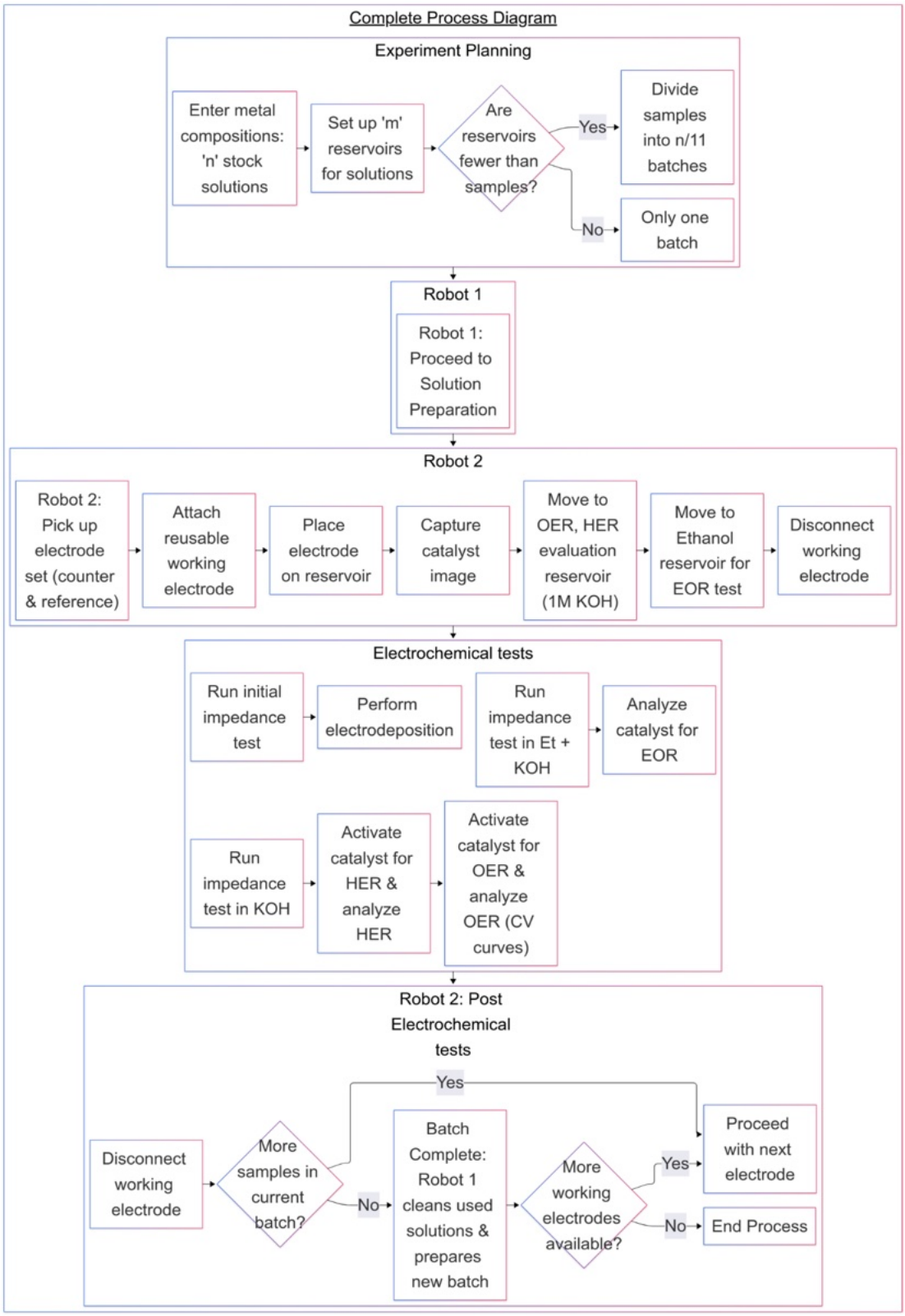

Figure 2-1 Complete process overview diagram.

The second SCARA robotic arm begins by retrieving the electrode holder, equipped with the counter electrode (CE) and reference electrode (RE), and then maneuvers it to the working electrode array to select a working electrode via magnetic attraction. Once the working electrode is secured to the holder, the arm positions the assembly into a designated solution tube for electrochemical deposition. The three-pin pogo connector automatically establishes electrical connections between the electrodes and the potentiostat. A Python script then activates the CHI electrochemical potentiostat to apply the required current or voltage, facilitating the deposition of metal ions from the solution onto the working electrode over a period of 10–20 minutes. Following deposition, the robotic arm retrieves the electrode holder, transfers it to a rinsing beaker to clean the electrodes, and proceeds to an imaging station to capture images of the electrode surface. Subsequently, the arm relocates the holder to a performance evaluation tube containing a test solution, such as 1 M KOH, where the electrochemical performance of the deposited catalyst is assessed (see below).

4) "Electrochemical evaluation of catalysts' performance". For electrochemical deposition, a Python script activates the CHI 660 potentiostat to control the process. Initially, an impedance test is conducted to measure the electrode's baseline impedance. Subsequently, a constant current or voltage is applied in the deposition solution, enabling metal ions to deposit onto the working electrode (WE) over a period of approximately 10–20 minutes. Following deposition, the electrode is rinsed, and an optical image is captured to document its surface. Robotic arm #2 then transfers the electrode assembly to an evaluation tube containing a test-specific solution—such as 1 M KOH for oxygen evolution reaction (OER) and hydrogen evolution reaction (HER)

tests, or 1 M ethanol + 1 M KOH for ethanol oxidation reaction (EOR) tests. In the evaluation solution, a second impedance test is performed, followed by cyclic voltammetry (CV) scans, typically 10 cycles, to activate the catalyst. After activation, performance evaluation scans (e.g., for OER or HER) are conducted, and the resulting data are recorded for subsequent analysis.

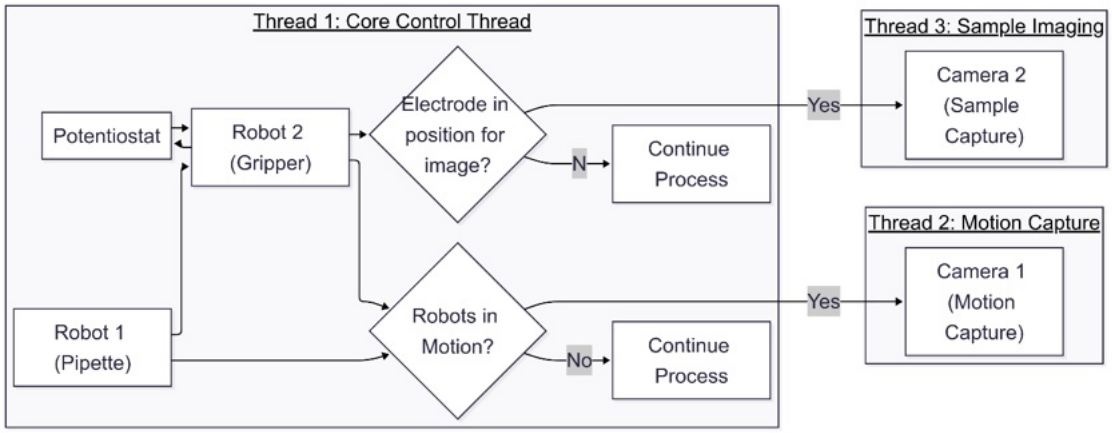

Figure 2-2 The core control thread of the autonomous system.

5) "To start the next sample". Upon completing the deposition and evaluation of one catalyst, the system proceeds to the next test. The working electrode is first detached from the electrode holder using a fixed-location scraper. The electrode is secured to the holder by two small magnets, allowing a gentle mechanical push from the scraper to release it. Robotic arm #2 positions the electrode holder near the scraper, which then removes the working electrode. Subsequently, a Python script checks whether additional samples require testing. If more samples are queued, the robotic arm moves to the next working electrode storage location to retrieve a new electrode and initiates the next experimental cycle. If no further samples remain, the Python program directs

Figure 2-3 Individual tools that construct the autonomous system.

robotic arm #1 to clear the solutions and prepare the system for a new batch of experiments, if necessary.

Figure 2-3 shows the individual tools that we need to build the autonomous system. Figure 2-3a are two SCARA robotic arms that are used for the solution dispersion and electrode manipulation. Figure 2-3b is the CHI 660E electrochemical potentiostat which will apply the potential or current for the catalysts deposition and evaluation. Figure 2-3c and Figure 2-3d are two cameras that we used to record and monitor the system's movements. Figure 2-3e is the pipette controller pump which will accurately suck in and out the solutions. Figure 2-3f is the gripper which will move the

electrode holder into different tubes. The bottom right in Figure 2-3g is the actuator that we used to build syringe in the early stage of our project.

a) b)

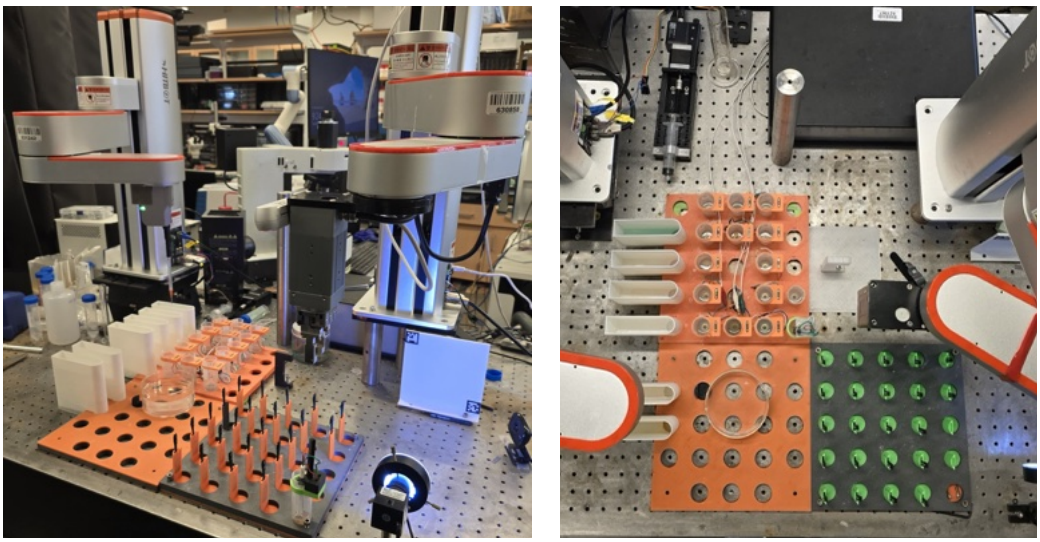

Figure 2-4 The entire autonomous catalyst screening system. a) Side view. b) Top view.

Figure 2-4 illustrates the complete autonomous experimental platform developed for this project, designed for high-throughput catalyst synthesis and screening. The system integrates two programmable robotic arms capable of precise and coordinated liquid handling, including reagent dispensing, sample mixing, and electrode rinsing. On the worktable, stock solution reservoirs are positioned alongside labeled deposition solution tubes and cleaning beakers to facilitate multi-step synthesis and electrode preparation. A custom-designed holder array securely accommodates working electrodes in a modular layout, enabling parallelized operations and systematic experimentation. An imaging station equipped with a mounted camera and LED lighting is positioned at the front of the setup to capture high-resolution visual data during or after synthesis. To the right of the platform, an electrochemical potentiostat is connected

to the electrodes for in-situ performance evaluation, providing real-time feedback for electrochemical characterization. A laptop serves as the central control unit, running

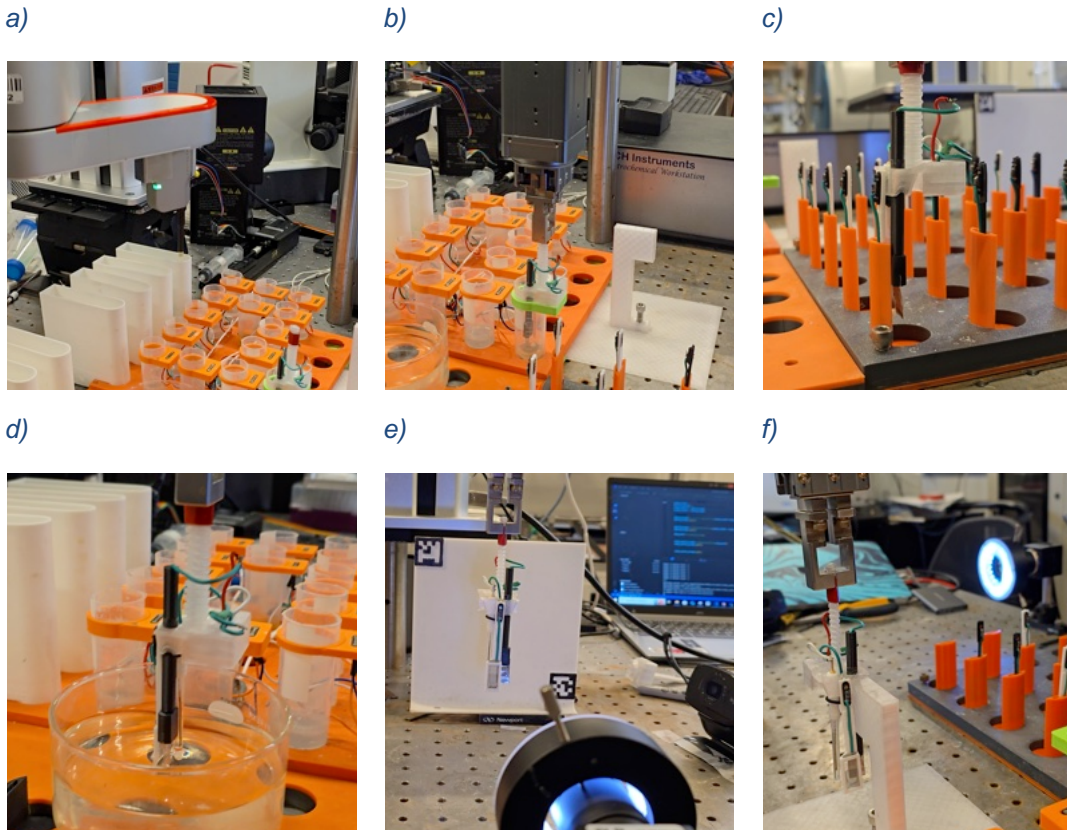

Figure 2-5 Parts of the complete process. a) Solution preparation. b) Electrode holder manipulation. c) Working electrode attachment d) Electrode washing. e) Sample imaging. f) Electrode detachment.

custom software that coordinates robotic actions, schedules experiments, and logs experimental data. The entire setup is mounted on an anti-vibration optical breadboard to ensure positional stability during automated operations. This configuration constitutes a fully automated, reconfigurable system capable of streamlining catalyst discovery with minimal human intervention.

2.2 Dispensing Solution Mixing Logic & Control

Our autonomous system is designed to synthesize and screen electrochemically deposited metal alloys for a variety of applications, with a focus on optimizing catalysts for electrochemical reactions such as the oxygen evolution reaction (OER). To accomplish this, the system automates the preparation of solutions containing different metal ions or precursors, ensuring precise and reproducible mixing tailored to specific alloy compositions. Figure 2-6 outlines the automated solution mixing procedure, which is a critical step in enabling high-throughput catalyst screening. The process begins with the system receiving a predefined dictionary specifying the desired chemical combinations. For instance, to screen ternary metal alloys like Ni-Co-Fe for OER performance, we input the targeted combinations of individual metal ion solutions (e.g., Ni^{2+}, Co^{2+}, Fe^{3+}) for each deposition tube. These combinations, along with the corresponding volumes for each metal ion solution, are determined prior to the experiment and stored in an array to guide the automation process.

The mixing procedure is orchestrated by a Python script that reads the array and systematically dispenses the metal ion solutions into the deposition tubes. To ensure efficiency, the system dispenses one type of metal ion solution across all tubes before switching to the next, minimizing the need for frequent syringe changes. For each tube, the program retrieves the required volume for the first metal ion solution. Given that our current syringe has a dispensing capacity of 1 mL per cycle, the script calculates whether the target volume exceeds this limit. If so, it divides the total volume into multiple 1 mL increments, plus any remaining fraction, and executes a loop to dispense the solution incrementally until the desired amount is achieved. Once the first tube is filled, the

system proceeds to the next tube, repeating the process until all tubes receive the first metal ion solution. The robotic arm then switches to the second metal ion solution, following the same dispensing sequence across all tubes, and continues this pattern for subsequent solutions as specified in the input array.

This automated mixing approach offers several advantages for catalyst screening. By precisely controlling the volume and composition of each solution, the system ensures consistency across experiments, reducing human error and variability that are common in manual preparation. The use of a predefined array also allows flexibility, enabling researchers to explore a wide range of alloy compositions without reconfiguring the hardware for each experiment. For example, adjusting the Ni:Co:Fe ratio in the input dictionary can generate diverse alloy candidates for OER testing, facilitating rapid iteration and optimization. Additionally, the sequential dispensing strategy optimizes throughput by streamlining the workflow, which is particularly valuable when screening large numbers of samples. To further enhance the system's capabilities, future iterations could incorporate multi-channel syringes or higher-capacity dispensers to reduce dispensing time for larger volumes, though the current setup already achieves reliable performance for lab-scale screening.

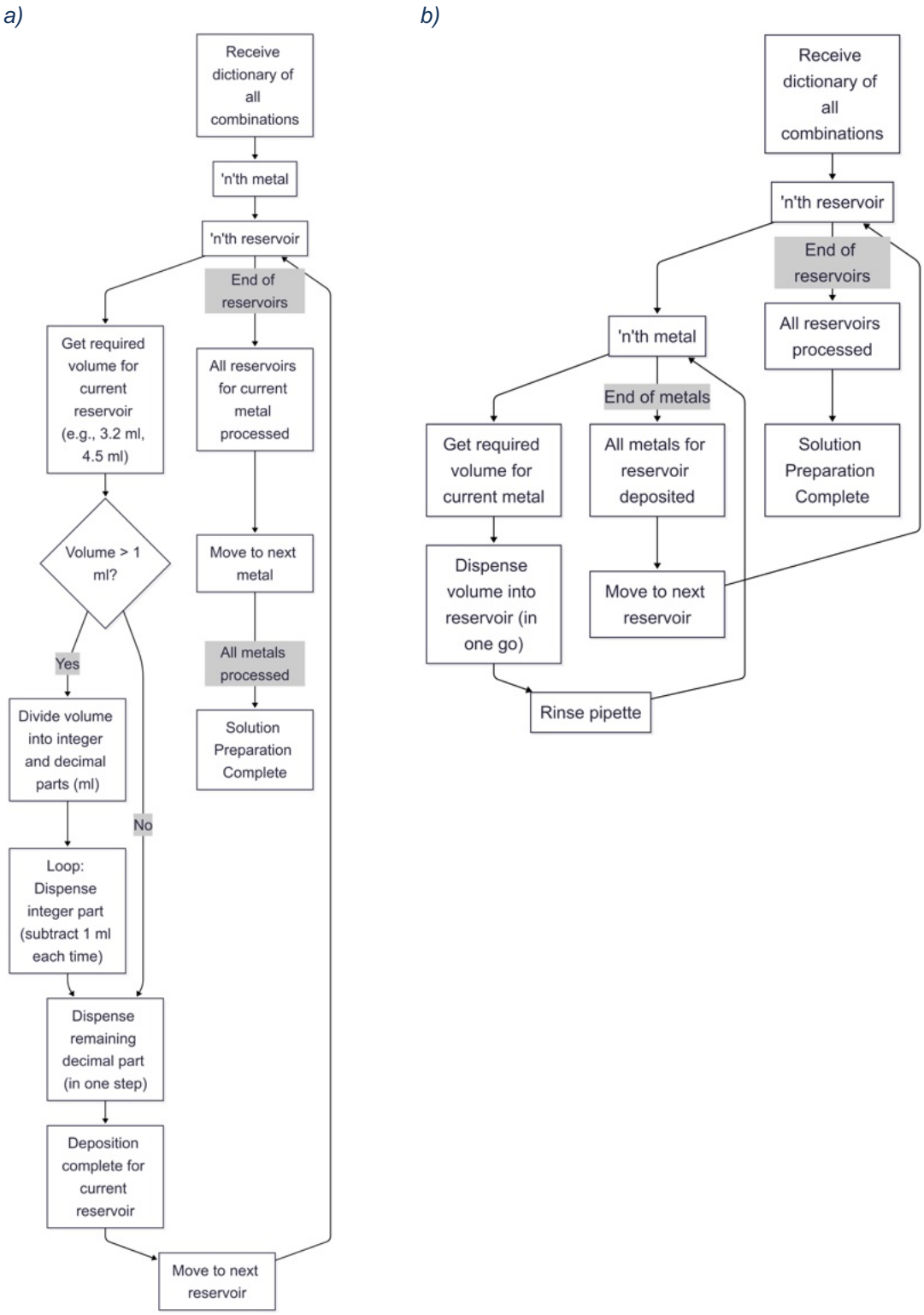

Figure 2-6. Automatic solution preparation process diagrams. a) Updated version with optimized sequence logic. b) Earlier version using a less efficient aspiration-dispense loop and linear reservoir traversal.

autonomous system, including robotic arms for electrode handling and electrochemical testing stations, as described in subsequent sections. This integration ensures that the prepared solutions are immediately available for deposition, maintaining a continuous workflow from mixing to performance evaluation. By automating this foundational step, our system not only accelerates the discovery of high-performing metal alloy catalysts but also lays the groundwork for scalable, data-driven exploration of complex chemical spaces, with potential applications in energy conversion, environmental remediation, and beyond.

2.3 Reservoir Hardware

To ensure precise and contamination-free dispensing of metal ion solutions, the autonomous system employs a carefully engineered stock solution reservoir module. Each stock solution reservoir is designed to hold a large volume (typically ≥50 mL) of precursor solution, minimizing the need for frequent refilling during high-throughput synthesis runs. These reservoirs are arranged in a fixed spatial configuration on the worktable to enable efficient access by the robotic arm, which manipulates a pipette connected to a motorized syringe pump.

The reservoirs are custom-fabricated using 3D-printed PLA or PETG materials, with thicker inner and outer walls to avoid leakages. Each container features a tight-fitting bottom that slots into the reservoir table ensuring a secured position during aspiration and reducing the risk of cross-contamination or collision.

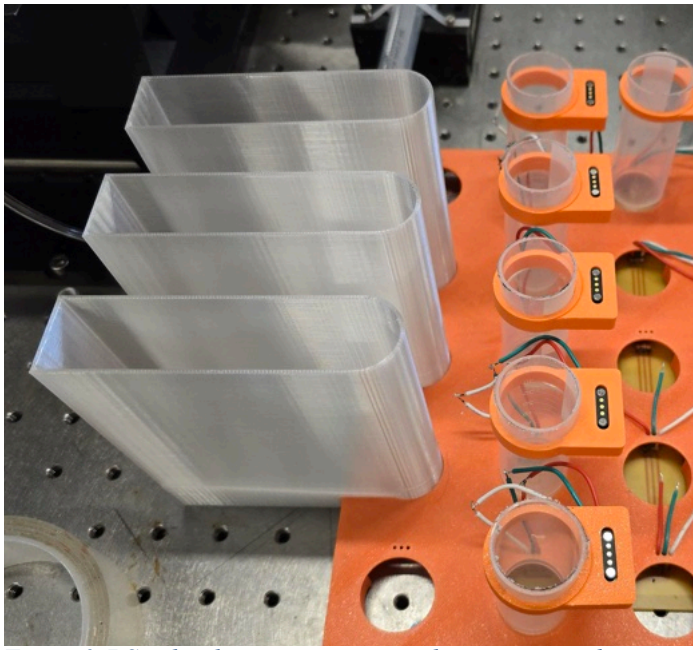

Figure 2-7 Stock solution reservoirs in the experimental setup.

To accommodate different alloy screening tasks (e.g., binary, ternary, or quaternary systems), the reservoir platform is modular. It can be expanded to hold more containers if additional metal ion solutions are required. During a typical experiment, the robot first positions the pipette above a designated reservoir, aspirates the required volume, and then proceeds to the target deposition tube. Between each aspiration cycle, the pipette tip is rinsed thoroughly in a dedicated reservoir using DI water to further ensure purity and reproducibility.

The fixed placement of the stock solution reservoirs also facilitates automated programming of the robotic arm trajectory. The Python control script maps the XY coordinates of each reservoir and incorporates precise movement commands that ensure consistent alignment with the pipette tip. This reduces positional error, prevents

splashing or spillage, and maintains the fidelity of each solution's composition during transfer.

Looking ahead, the design can be upgraded to integrate real-time volume sensing or flow-rate monitoring for each reservoir. This would allow for automated alerts when solution levels are low or if flow rates deviate from expected values, further improving the reliability of the system. For more scalable deployments, future iterations may also support reservoir heating or stirring modules to accommodate temperature-sensitive or unstable stock solutions.

In summary, the current reservoir design balances simplicity, functionality, and adaptability—enabling our self-driving lab to deliver accurate and consistent precursor volumes critical to the reproducibility of electrocatalyst synthesis.

2.4 Liquid-Handling Hardware Evolution

In the early phase of system development, solution dispensing was achieved using a custom syringe pump built on a Zaber LSQ series linear stage. The stage offered high positional accuracy (up to 35 μm) and repeatability (<2 μm), theoretically providing precise volume control when coupled with a 20 mL or 30 mL generic syringe. A calibration multiplier was manually derived to map linear displacement to fluid volume aspirated or dispensed. This system was mounted onto the worktable and connected via tubing to the SCARA robotic arm's end effector, allowing the robot to access deposition tubes and reservoirs as needed.

While this setup worked well for initial testing, several challenges quickly emerged. The main issue stemmed from the use of compressible air in the long tubing

that connected the syringe to the pipette tip. Backflow effects became noticeable when aspirating small volumes or operating at high speeds, due to air compressibility and elasticity of the tubing. We experimented with different materials—including silicone and PTFE tubing—to mitigate these effects. PTFE, while hydrophilic, still required priming with DI water to minimize compressibility. However, this workaround introduced risks of cross-contamination and did not guarantee consistent performance over multiple cycles.

Additionally, although the 30 mL syringe allowed larger solution transfers per stroke, this did not translate into greater precision for small-volume applications such as ternary or quaternary alloy preparation. Low-volume dispensing was particularly sensitive to pressure variations, leading to inconsistent aspirated volumes and unreliable mixing ratios. Slowing down the linear stage movement helped reduce error, but at the cost of significantly increased preparation time—especially when scaling up the number of samples.

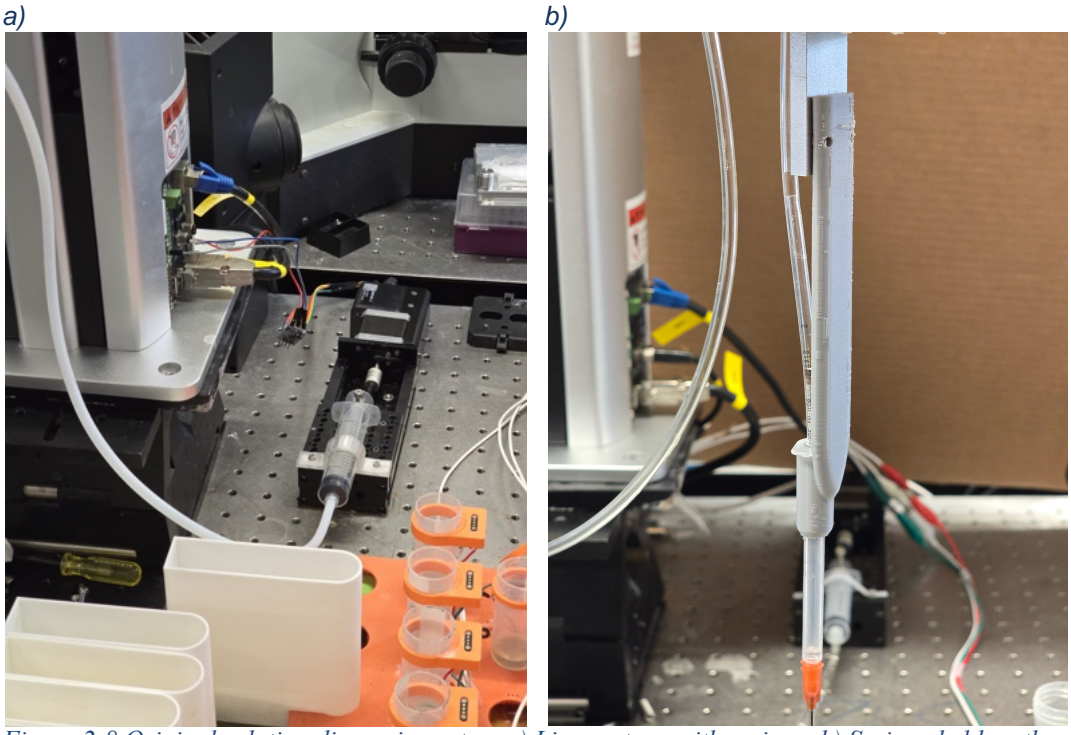

Figure 2-8 Original solution dispensing setup. a) Linear stage with syringe. b) Syringe held on the end effector of the robot.

Figure 2-8 shows the original setup: the Zaber linear stage mounted with a syringe pump, and the long tubing connection to the robot-mounted pipette. The limitations of this design became a bottleneck as we aimed for high-throughput, high-precision workflows.

To resolve these issues, we transitioned to an industrial digital pipette system, directly integrated with the SCARA controller via RS-485 using the Modbus ASCII protocol. The pipette provides microfluidic-level accuracy with error margins on the order of a few microliters—an essential feature for reproducible mixing of multiple metal ion solutions. Although the digital pipette has a smaller maximum volume (1 mL), its precise control and tight integration with our dispensing algorithm (which avoids

switching between stock reservoirs between every aspiration) has greatly improved overall efficiency and throughput.

This shift not only eliminated the mechanical complexity of the linear stage system but also ensured accurate and contamination-free fluid handling. The Zaber stage has since been phased out of the setup, as its functionality was fully replaced by the digital pipette system.

In summary, the linear-stage-based syringe pump provided a flexible starting point but was ultimately limited by pneumatic instability and speed–accuracy trade-offs. The adoption of a digitally controlled pipette marks a key evolution in our autonomous liquid handling system, enabling precise and consistent solution preparation—particularly for high-complexity alloy compositions.

CHAPTER 3 HARDWARE & FIXTURE DESIGN

3.1 Electrode Holder Evolution

The first version of the electrode holder featured a single set of counter, reference, and working electrodes connected directly to the potentiostat using thin wires. The entire electrode set was manipulated by the second SCARA robotic arm via a 3D-printed holder made from PLA, printed vertically. While it was possible to replace the working electrode between tests, the process, though quick, introduced inconsistency. Ensuring the stainless-steel mesh was clipped in the exact same position each time proved difficult and compromised repeatability.

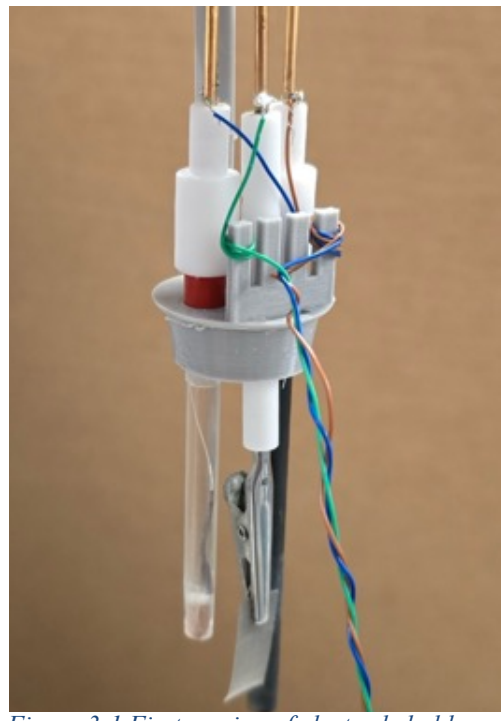

Figure 3-1 First version of electrode holder.

The thin wired connections also posed major mechanical challenges. The wires would often become entangled during robotic manipulation or even rip off entirely, especially if the arm path deviated slightly. In worst-case scenarios, this would crash the system and halt operations. The initial gripper interface was a straight cylindrical pillar, which had alignment issues inside the robot's parallel gripper. This was soon

revised into a diamond-shaped profile that naturally fit the gripper orientation. Later improvements introduced ribbed features to enhance mechanical grip.

Due to these limitations, the setup was constrained to single-run automation. Each sample had to be prepared and evaluated individually, which bottlenecked the entire throughput potential of the autonomous platform.

To eliminate the problems caused by wired connections, the second design iteration replaced all wiring with magnetic pogo pin connectors. These pogo pins were press-fitted into a 3D-printed holder mounted next to each electrochemical reservoir. The robot-mounted electrode holder carried the complementary magnetic contacts.

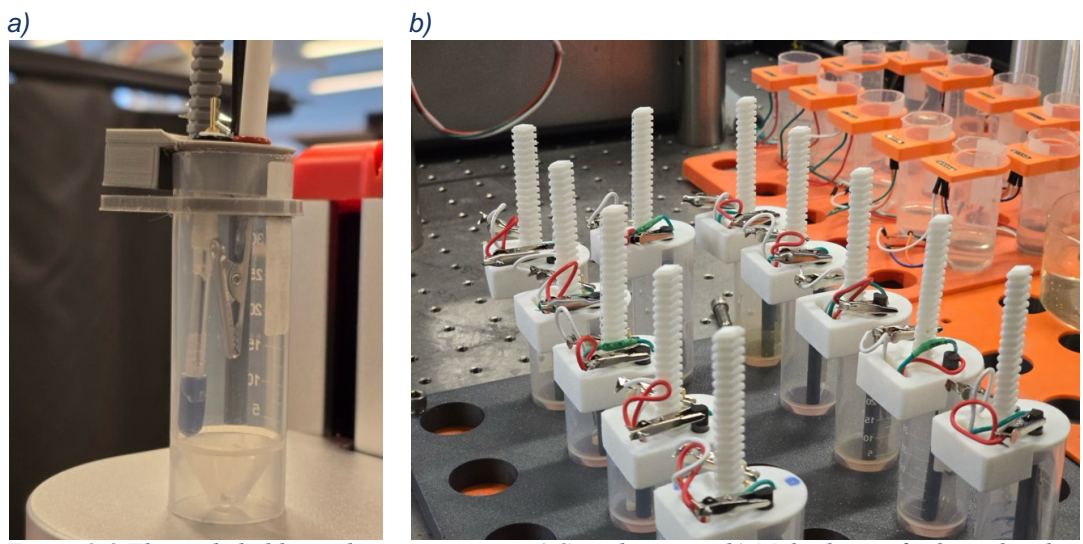

Figure 3-2 Electrode holder with magnetic pins. a) Singular setup. b) Multiple sets for large batch of experiments.

Reliable electrical contact was achieved by leveraging both the repeatability of the SCARA robot and the self-aligning property of magnetic attraction. When the electrode holder was lowered into place, the magnetic force would draw the pogo pins into perfect alignment, ensuring robust and consistent contact with minimal effort. This

improvement drastically increased the system's mechanical stability and enabled more agile robotic motion without the risk of wire entanglement.

3.2 Printed-circuit backplane

To cut down the bundle of point-to-point jumpers used in early prototypes (Figure 3-3a), we added a single-layer PCB under the reservoir plate (Figure 3-3b). The board is produced entirely in-house: a laser-printed transparency carrying the trace artwork is UV-exposed onto presensitized copper-clad, then etched in $FeCl_3$ and drilled.

At each tube the traces terminate in short pigtail leads that climb the reservoir wall and end in a spring-clip contact mounted just below the rim (Figure 3-3b). When the SCARA arm lowers the electrode holder, pogo pins on the holder land on the clip, closing the three-wire circuit (WE, CE, RE). Lifting the holder breaks the connection; no connectors or magnets are embedded in the PCB itself.

The PCB reduced the number of failure points. Long, flexing jumpers have been replaced by fixed copper traces.

Simple scaling —as the number of reservoirs grows, new traces are added to the board layout instead of threading individual wires through the workspace.

In effect, the reservoir plate now functions as a passive, plug-and-play distribution bus: the robot only has to "set the holder down" to complete a reliable, low-noise connection for every experiment.

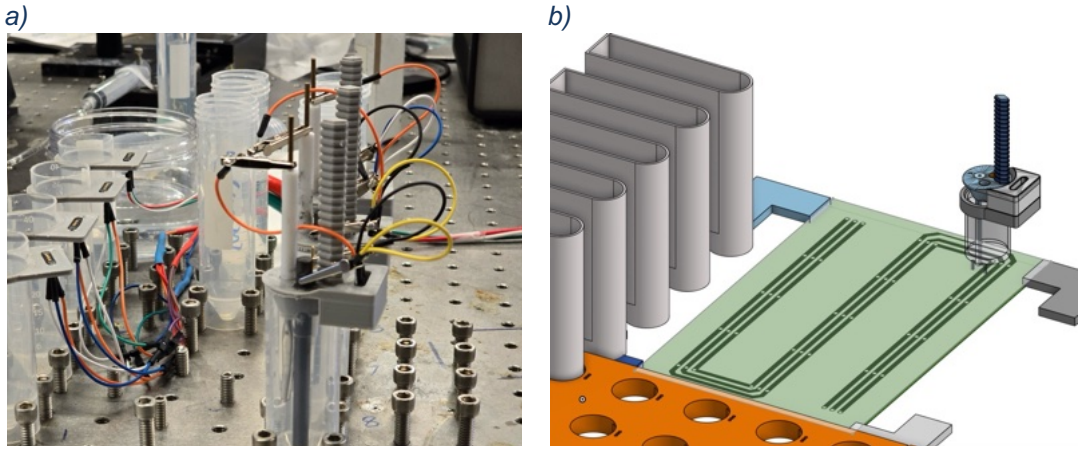

Figure 3-3 a) Initial prototype with magnets and long wires. b) 3D model of the PCB beneath the tube stand.

3.3 Multi-Reservoir System with Swappable Electrode Bundles

The third iteration expanded the system's scalability by introducing multiple pogo-pin-equipped reservoirs and independent electrode holders. Each holder carried a fresh stainless-steel mesh working electrode, enabling the robot to perform a complete round of synthesis and evaluation steps sequentially across 11 reservoirs.

However, while this version improved batch throughput, it introduced a new layer of complexity. Each electrode set still required its own reference and counter electrodes. Maintaining 11 sets of Ag/AgCl reference electrodes became impractical over time. Their performance would drift as the internal KCl solution degraded, demanding periodic maintenance or replacement. The cost and effort associated with keeping multiple platinum counter electrodes in service further reduced the system's

long-term viability. As such, this version was functionally effective but unsustainable for routine use or scaling.

3.4 Final Modular Electrode Holder Design

To address these challenges, the final design iteration modularized only the working electrode. A slot was introduced into the 3D-printed electrode holder to accommodate a switchable stainless-steel mesh, which could be detached and replaced without modifying the reference or counter electrode. A guide system was also printed to ensure precise robot-assisted placement of new working electrodes.

This design enabled the reuse of a single, stable set of reference and counter electrodes across all tests, greatly reducing the burden of calibration and maintenance. The change not only cut costs—especially for the platinum counter electrodes—but also enhanced repeatability, as all samples were tested under the same electrode field configuration.

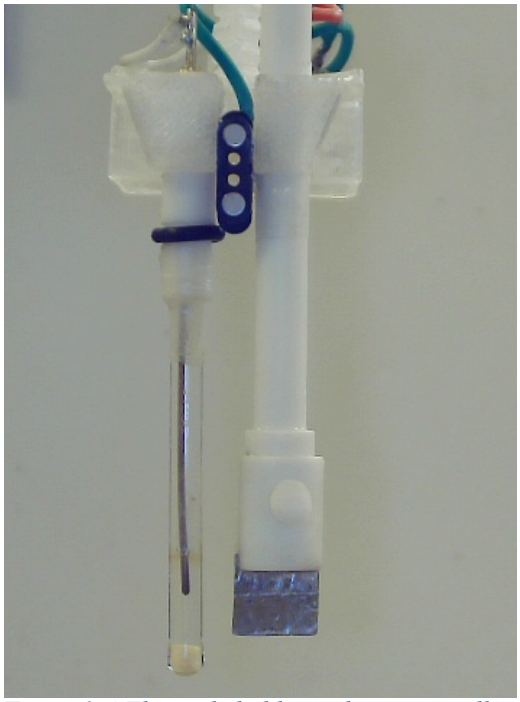

Figure 3-4 Electrode holder with magnetically attaching working electrode.

Mechanically, earlier versions of the holder would often fail at the gripper interface due to stress concentration along 3D-printing layer lines. The solution was to switch the print orientation to horizontal, improving durability and eliminating breakage

during repeated manipulation cycles. With this new modular configuration, the system could reliably perform full rounds of electrochemical synthesis and evaluation while minimizing both operational complexity and part replacement frequency.

3.5 Transition to Working Electrode Optimization

With the core electrode holder architecture stabilized, the focus shifted to optimizing the working electrode module itself. Previous designs suffered from inconsistent repeatability due to imprecise electrode placement and degradation in contact quality. These inconsistencies, in part, stemmed from variability in electric field distributions when different electrode geometries or placements were used between runs.

Optimizing the working electrode interface reduced the variability in deposition behavior and improved the reproducibility of electrochemical data such as overpotential and CV curves. The modular system, aided by alignment guides and robust mechanical interfaces, laid the foundation for the next design iteration focused on maximizing reliability, minimizing contamination, and improving field consistency during deposition and evaluation.

CHAPTER 4 WORKING ELECTRODE DESIGN OPTIMIZATION

4.1 Importance of Orientation and Positioning in Repeatability

In electrochemical experiments such as OER (Oxygen Evolution Reaction), even slight variations in electrode positioning can lead to significant inconsistencies in results. To quantify this effect, a systematic study was conducted to examine the influence of the orientation, rotation, and placement angle of the stainless-steel mesh working electrode. All tests were carried out using the same counter and reference electrodes, and the working mesh was reused post-activation without altering any other experimental parameters.

The working electrode was tested under the following conditions:

- **Top row (Left to Right):**
  - 0° axial rotation
  - 90° axial rotation
  - 0° rotation with 30° left bend
- **Bottom row (Left to Right):**
  - 0° axial rotation with 30° rotation
  - 90° axial rotation with 30° right bend
  - 90° axial rotation with 30° left bend
  - 0° axial rotation with 60° left bend

Despite identical electrochemical settings, the CV scans showed variations in overpotential on the order of at least 10 mV at fixed current densities across different

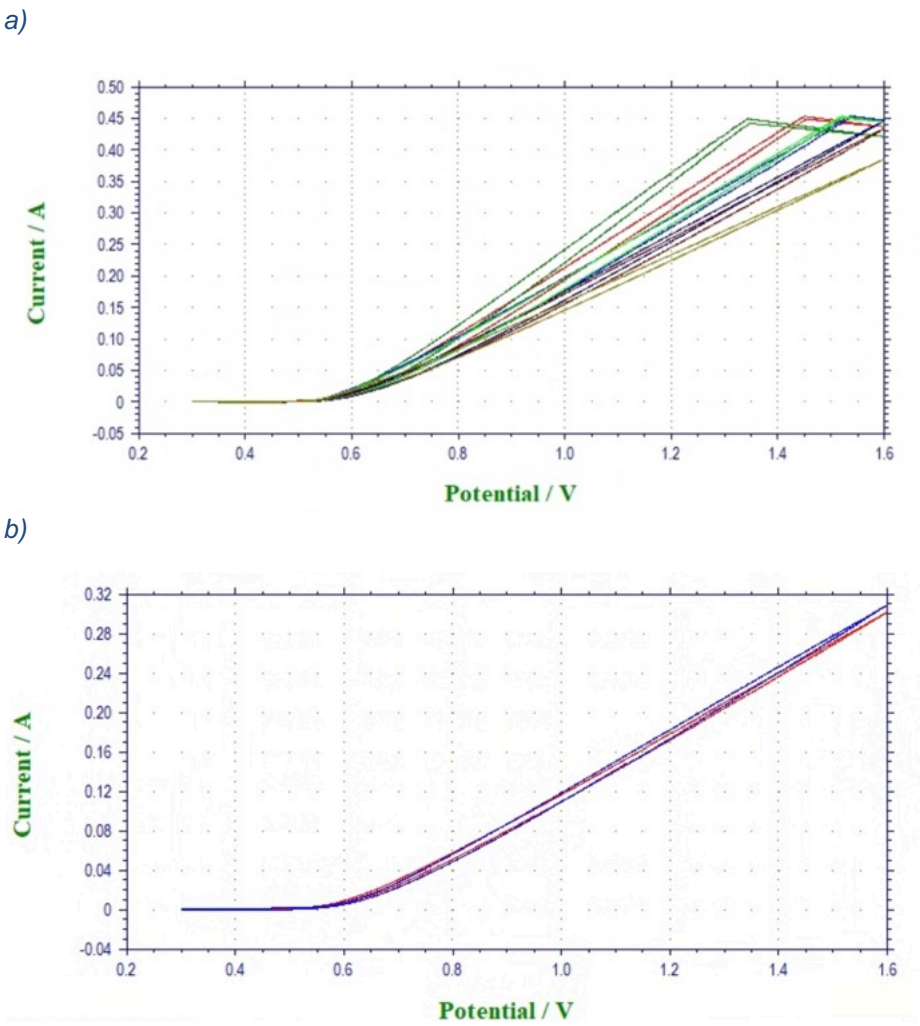

Figure 4-1 CV curves comparing two versions of working electrodes clips. a) Traditional design with stainless steel clips to attach mesh. b) Newest design with standardized orientation.

configurations. These discrepancies highlighted the critical importance of consistent working electrode placement for achieving repeatable and reliable data.

4.2 First Modular Frame Design

To address this variability, a modular frame design was created to enforce uniformity in mesh orientation, depth, and distance from the counter electrode. The initial version used a 3D-printed foldable frame clip with a conducting wire embedded into the holder body. The clip allowed stainless steel mesh to be slotted in and folded into position, ensuring alignment through mechanical constraints.

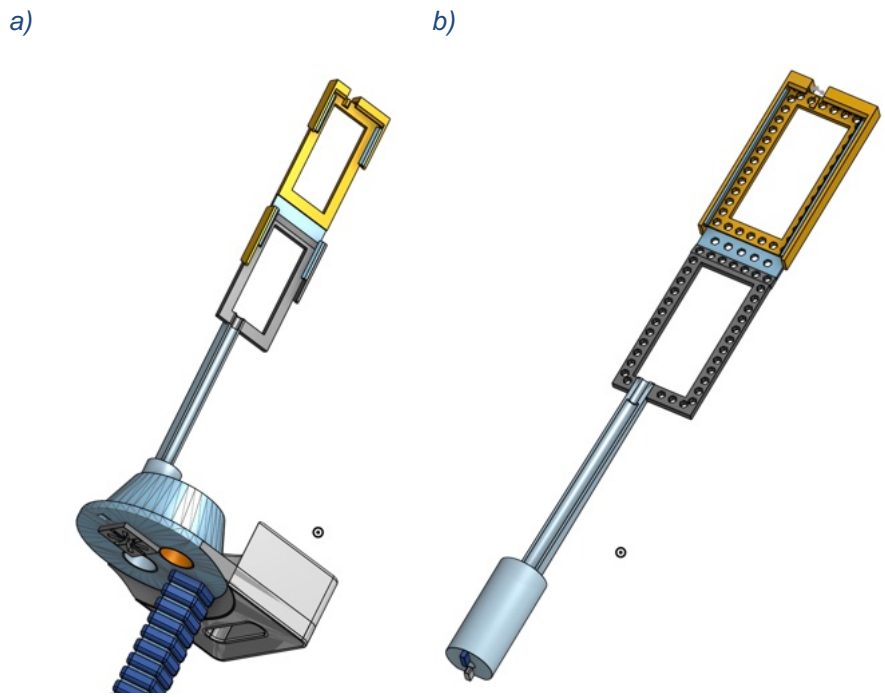

Figure 4-2 Working electrode clip designs.

Although this foldable frame offered modularity, it had serious mechanical drawbacks. The hinge mechanism degraded after a few cycles of use, either breaking or becoming too loose to hold the mesh securely. Multiple materials and design parameters were evaluated to maintain good electrical contact while enabling easy interchangeability:

- **PLA:** Fragile; broke after a few insertions due to hinge fatigue

- **PETG:** Too rigid; layer bonding was inconsistent, leading to delamination
- **TPU:** Too flexible; contact was unreliable
- **PP (Polypropylene):** Optimal balance between rigidity and flexibility; provided reliable contact and repeated mesh switching

4.3 Bubble Formation and Redesign

Although the PP-based clip resolved electrical contact issues, new challenges emerged during long-term OER testing in KOH solution. The loosely fitting frame would sometimes trap gas bubbles—particularly along the inner edges of the mesh—

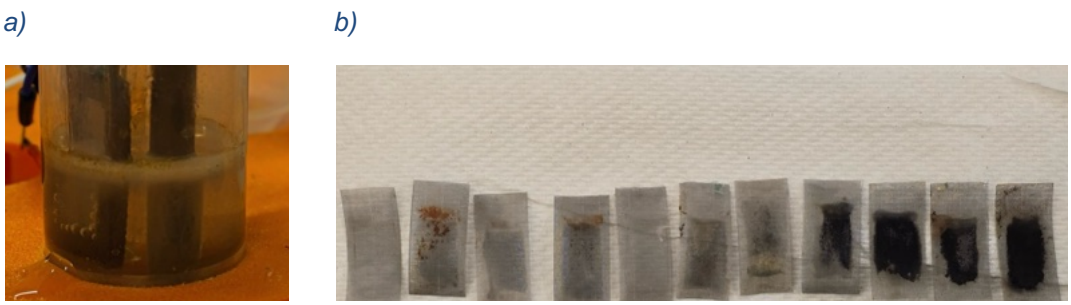

Figure 4-3 Bubble formation problem. a) Bubble formation during OER. b) Uneven deposition on top of stainless steel mesh.

leading to uneven deposition and oxidation patterns. These inconsistencies were clearly visible in CV scan deviations and observed physically in Figure 4-3.

To mitigate this, the design was revised to eliminate the hinge altogether. The new version, shown in Figure 4-4, consisted of a sturdy single-piece frame with a precise slit for sliding in the stainless-steel mesh. This configuration significantly reduced bubble entrapment and also minimized mechanical flexing. The rigid edges ensured constant contact pressure with the conducting wire embedded in the holder, maintaining a stable electrical connection throughout.

4.4 Final Integration with Electrode Holder

Once a mechanically stable and electrically consistent working electrode frame was achieved, it was integrated with the existing modular electrode holder via a

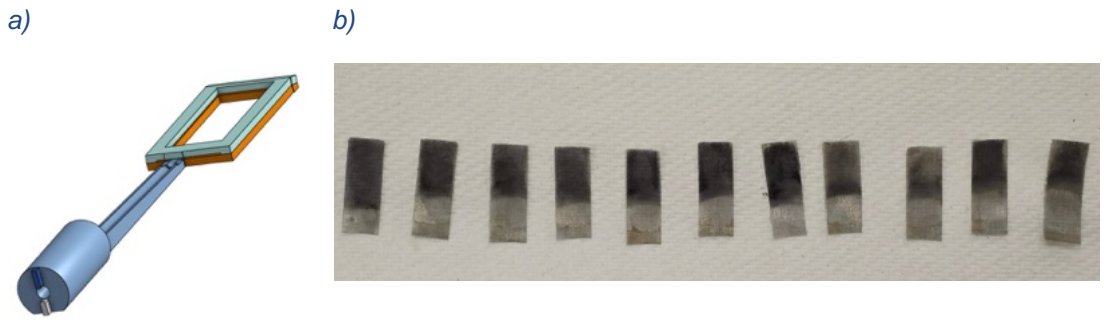

Figure 4-4 Improved design. a) Working electrode clip without the hinge mechanism. b) Deposition results using new design.

magnetic pogo pin connection (see Figure 3-2). This final configuration maintained the same counter and reference electrodes for all samples, streamlining the entire process and reducing both cost and maintenance.

An additional improvement was the thickening of the frame walls to prevent warping and flexing during handling or insertion of the wire. This structural enhancement improved alignment precision and reinforced the consistency of contact depth and electrode exposure.

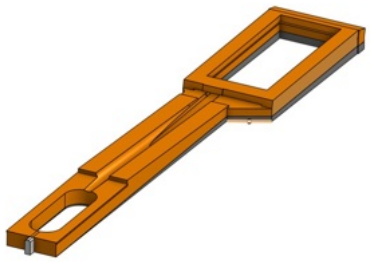

Figure 4-5 Working electrode clip with reinforced walls

The optimized working electrode design provided:

- High reproducibility across samples
- Minimal performance variation

- Quick interchangeability without disturbing the electrode setup
- Significantly reduced material degradation and maintenance cycles

This design refinement plays a critical role in the reliability and scalability of the autonomous electrochemical platform, ensuring that subtle differences in performance reflect material properties rather than experimental artifacts.

CHAPTER 5 AUTOMATED DATA ANALYSIS AND VISUALIZATION

5.1 Pipeline Overview & Motivation

In high-throughput catalyst screening workflows, generating large volumes of electrochemical data is only the first step. Extracting insights from these datasets requires consistent, scalable, and efficient post-processing. To this end, we developed a Python-based data analysis framework that automatically parses experimental output folders, applies IR compensation, normalizes current densities, and visualizes key performance metrics across varying catalyst compositions. This automation is critical for enabling meaningful comparisons across dozens of samples, especially when data is collected from ternary and quaternary compositions using techniques like cyclic voltammetry (CV), chronopotentiometry (CP), and electrochemical impedance spectroscopy (EIS).

5.2 Processing Pipeline

The core of the analysis is a modular script that accepts a data folder as input and executes the following steps:

1) **Impedance Parsing:** Files matching impedance patterns are parsed to extract Z' and phase values using a function These values are stored in dictionaries indexed by the composition.

2) **Data Type Classification:** Experimental files are classified into CV, CP, and EIS based on header patterns and processed accordingly.

3) **IR Compensation and Normalization:** CV potential data is IR-compensated using the Z' values and adjusted relative to the reference electrode (RHE). Current values are normalized by electrode area, which can be specified or defaulted.

4) **Performance Extraction:** For each sample, the script identifies the potential at a fixed current density (e.g., 10 mA/cm² for OER or -10 mA/cm² for HER), allowing direct comparison of performance metrics across compositions.

5) **Ternary Plot Generation:** The overpotential or HER/OER potential values are plotted as heatmaps or scatter plots using the python-ternary package. Multiple interpolation techniques (RBF, kriging, IDW, nearest neighbor) are supported.

6) **Time-Series Visualization:** CP curves are plotted to show time-vs-potential trends, highlighting catalyst stability and behavior under prolonged operation.

7) **Overlay Comparisons:** CV sweeps for ethanol oxidation (EOR), HER, and OER are plotted in overlapping formats to visually compare electrochemical performance across different catalyst classes.

5.3 Interpolation Methods for Ternary Mapping

To convert discrete catalyst compositions into continuous heatmaps, the system supports a variety of interpolation methods:

1) **Nearest Neighbor:** Fastest, but less smooth.
2) **Radial Basis Function (RBF):** Gaussian and multiquadric kernel variants provide smooth gradients.
3) **Inverse Distance Weighting (IDW):** Weighted averaging based on proximity.

4) **Ordinary Kriging:** Incorporates spatial correlations via variograms.
5) **Linear Interpolation (Barycentric):** Uses geometric triangulation for local fitting.

These methods enable the visualization of electrochemical performance across compositional space, supporting both discovery and fine-tuning of optimal alloy compositions.

5.4 Performance Metrics and Visualization

The pipeline automatically computes and visualizes:

1) **Overpotential at 10 mA/cm² (OER)**
2) **Potential at -10 mA/cm² (HER)**
3) **Potential at 10 mA/cm² (EOR)**
4) **Chronopotentiometry trends**
5) **Ternary heatmaps and scatter plots**
6) **Overlapping CV plots (Sweep 1 and 2)**

Each plot is exported to a folder inside the experiment directory, allowing quick access for documentation, presentation, or further analysis.

5.5 Example Output and Applications

The script has been tested across datasets including NiFe, NiFeCo, and NiMoP compositions. It successfully generated ternary maps showing OER and HER performance trends, enabling identification of optimal regions for further exploration.

Overlay plots further revealed the impact of composition on CV curve shape and onset potentials.

5.6 Scalability and Reusability

The pipeline is designed to work across any dataset that follows the naming convention for concentration-encoded filenames. It is easily extendable to include new electrochemical techniques or electrode geometries. This script forms the analytical backend for our self-driving lab, ensuring that each automated synthesis is followed by equally automated evaluation.

This tool not only improves the reproducibility and objectivity of performance evaluation but also significantly reduces the time required to go from data collection to insight generation.

CHAPTER 6 CATALYST SCREENING RESULTS

This chapter summarizes the electrochemical performance of various bimetallic and trimetallic catalyst compositions synthesized and tested using the autonomous platform. The results are organized into two major sections: bimetals (NiFe and NiCu) and ternary compositions (NiFeCo and NiMoP). For each composition set, we present chronopotentiometry (CP), cyclic voltammetry (CV), overpotential extraction, and ternary mapping results to assess activity trends.

6.1 Bimetallic Catalysts

6.1.1 NiFe Series

Chronopotentiometry (CP) tests across 11 Ni:Fe ratios from 0:10 to 10:0 revealed distinct trends in potential stability during constant current operation. As seen in Figure 6-1, samples with intermediate Ni content (e.g., 4:6, 5:5) showed more stable

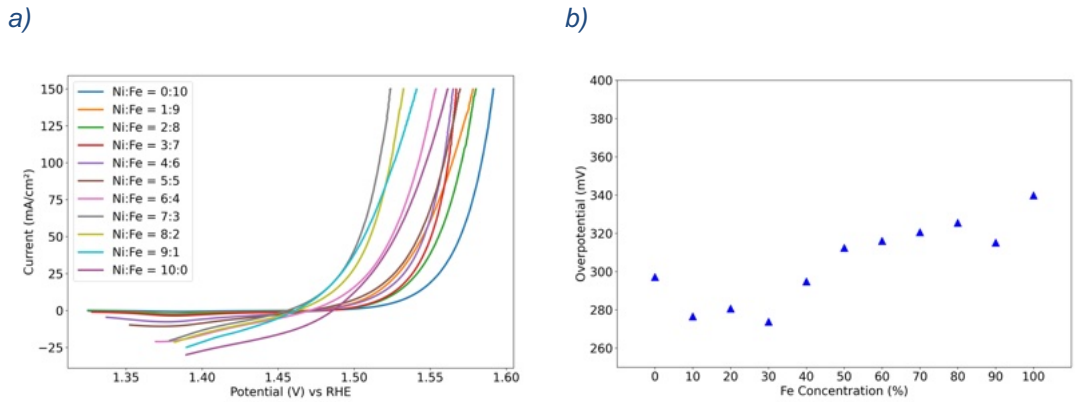

Figure 6-1 NiFe results. a) CV scans with different NiFe ratios. b) Overpotential at 10 mA/cm²

potentials, whereas edge cases like 0:10 or 10:0 exhibited more fluctuation and higher overpotentials.

The CV sweeps Figure 6-1a show a consistent shift in onset potential as Fe content increases. The highest current densities were achieved by mid-range Ni:Fe ratios. Overpotential extracted at 10 mA/cm² Figure 6-1b shows a clear minimum near 20-30% Fe content, suggesting an optimal synergy between Ni and Fe for OER activity.

6.1.2 NiCu Series

For NiCu, CV plots Figure 6-2a indicate lower activity for Cu-dominant compositions. The overpotential trend Figure 6-2b shows a monotonic increase with increasing Fe content, highlighting reduced synergy between Cu and Fe in this bimetallic system compared to NiFe.

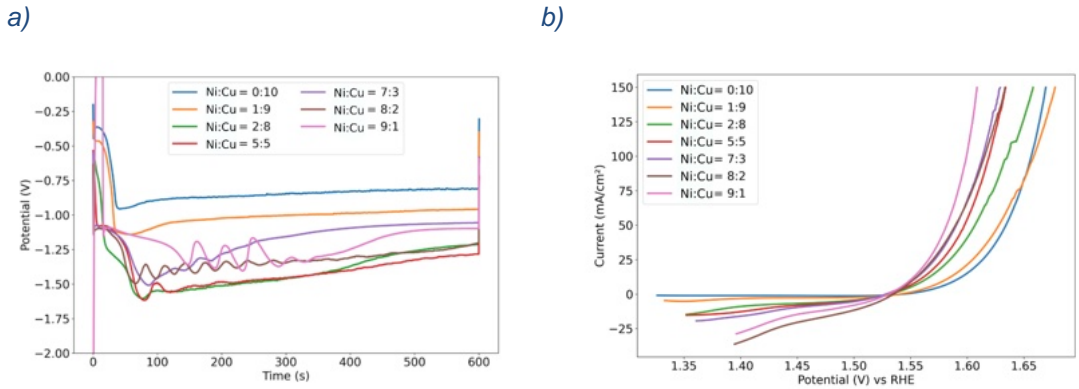

Figure 6-2 NiCu results. a) CV scans with different NiFe ratios. b) Overpotential at 10 mA/cm².

6.2 Trimetallic Catalysts

6.2.1 NiFeCo

The NiFeCo trimetallic system was extensively mapped using 66 unique compositions. CV plots in Figure 6-3a show a dense matrix of performance curves across the ternary space.

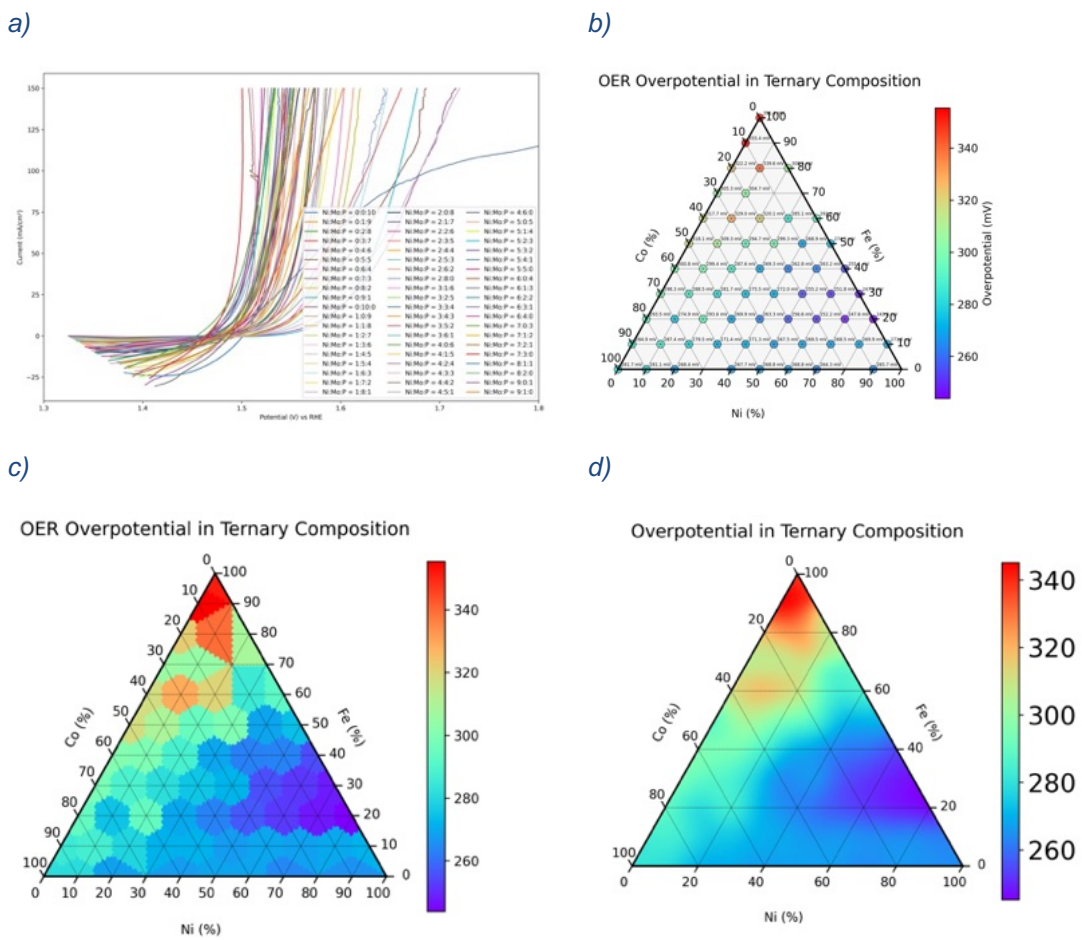

Figure 6-3 NiFeCo results. a) CV scans with different NiFeCo ratios. b) Ternary plot with overpotential at 10 mA/cm^2. c) Ternary plot with nearest neighbor interpolation. d) Ternary plot with radial basis function interpolation.

Ternary plots in Figure 6-3 illustrate OER overpotential distribution across the compositional landscape. The raw scatter (Figure 6-3b), interpolated heatmap (Figure 6-3c), and another interpolation (Figure 6-3d) all point to a compositional region rich in Ni and moderate in Fe as optimal, while high Co content leads to increased overpotentials. An independent batch prepared at 4 mA constant current and dried overnight produced a virtually identical map (Figure 6-4), confirming the robustness of the observed trend.

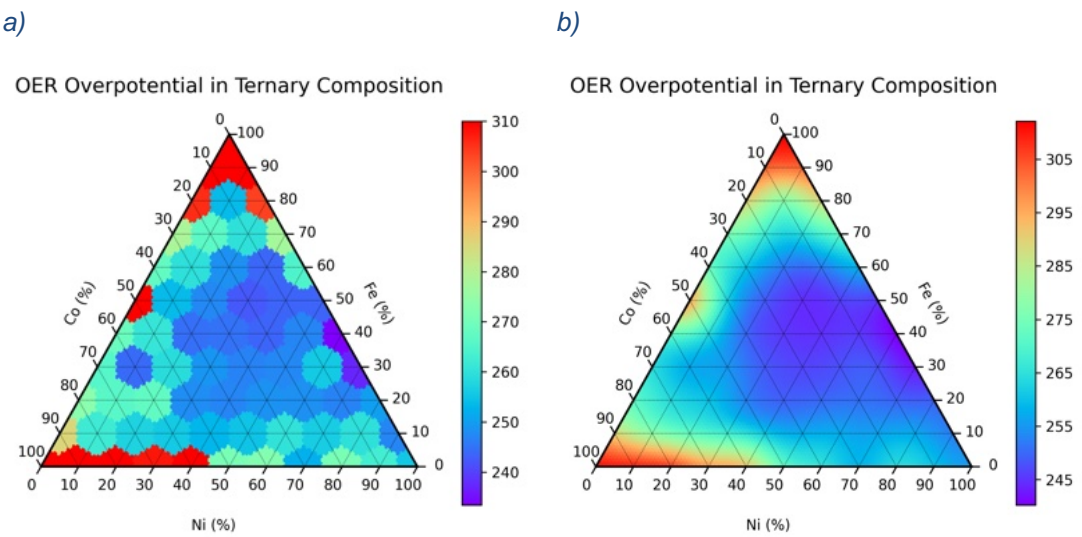

Figure 6-4 NiFeCo results from a different batch. a) Nearest neighbor interpolation. b) Radial basis function interpolation (RBF)

6.2.2 **NiMoP**

Similar testing was conducted for the NiMoP system, with 36 unique compositions. CV curves in Figure 6-6a demonstrate a broad distribution of behaviour.

Figure 6-6a presents OER ternary maps at 100 mV/s scan rate. The optimal performance zone appears in Ni-rich regions, with Mo and P offering minor enhancements.

Figure 6-5 summarizes HER performance. HER ternary maps show clear regions of lower potential (more negative) values in Ni-dominant compositions. Interpolated maps confirm that both Mo and P contribute positively to HER activity, particularly in balancing Ni's surface properties.

These results highlight the power of high-throughput, automated synthesis and characterization for materials discovery. The observed trends not only validate the system's ability to detect electrochemical differences with high resolution but also identify promising compositional domains for future catalyst development.

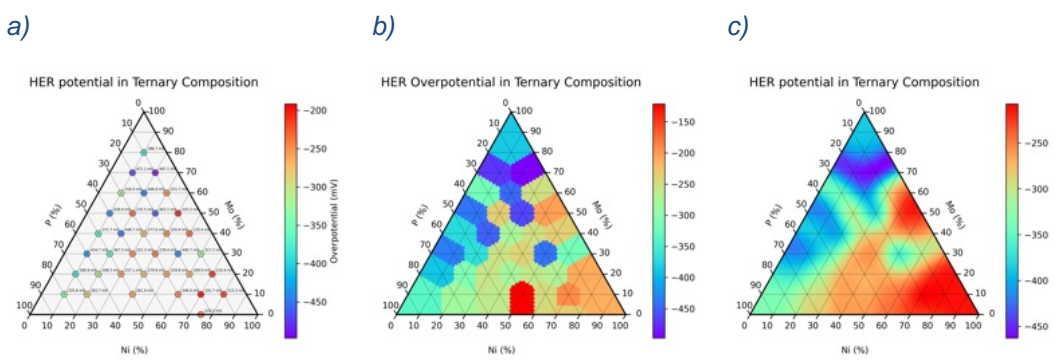

Figure 6-5 NiMoP HER results for overpotential at 10 mA/cm^2. a) Scatter plot. b) Plot with nearest neighbor interpolation. c) Plot with radial basis function interpolation.

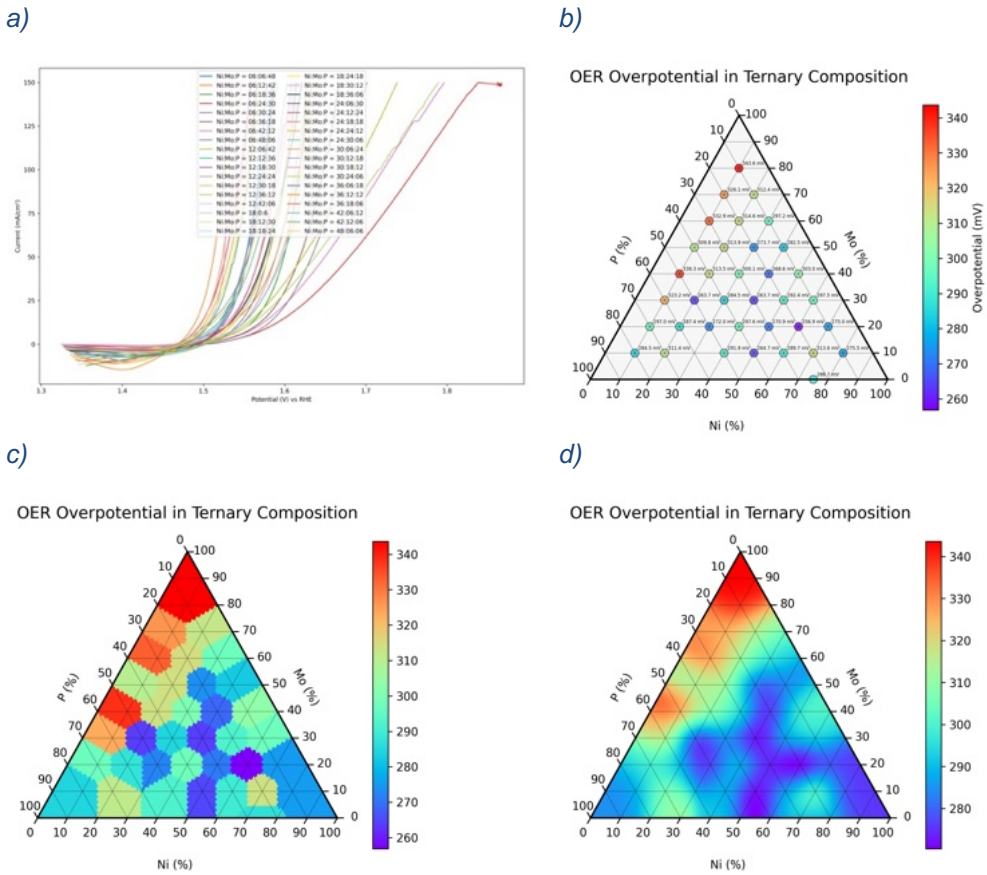

Figure 6-6 NiMoP OER results. a) CV scans with different NiMoP ratios. b) Ternary plot with overpotential at 10 mA/cm^2. c) Ternary plot with nearest neighbor interpolation. d) Ternary plot with radial basis function interpolation

REFERENCES

(1) Dobrzański, L. A. Significance of Materials Science for the Future Development of Societies. *J. Mater. Process. Technol.* **2006**, *175* (1), 133–148. https://doi.org/10.1016/j.jmatprotec.2005.04.003.

(2) Cottrell, W. F. *Energy and Society : The Relation between Energy, Social Change, and Economic Development*; Greenwood Press, 1970.

(3) Roco, M. C.; Bainbridge, W. S. The New World of Discovery, Invention, and Innovation: Convergence of Knowledge, Technology, and Society. *J. Nanoparticle Res.* **2013**, *15* (9), 1946. https://doi.org/10.1007/s11051-013-1946-1.

(4) Salonitis, K.; Pandremenos, J.; Paralikas, J.; Chryssolouris, G. Multifunctional Materials: Engineering Applications and Processing Challenges. *Int. J. Adv. Manuf. Technol.* **2010**, *49* (5), 803–826. https://doi.org/10.1007/s00170-009-2428-6.

(5) Tabor, D. P.; Roch, L. M.; Saikin, S. K.; Kreisbeck, C.; Sheberla, D.; Montoya, J. H.; Dwaraknath, S.; Aykol, M.; Ortiz, C.; Tribukait, H.; Amador-Bedolla, C.; Brabec, C. J.; Maruyama, B.; Persson, K. A.; Aspuru-Guzik, A. Accelerating the Discovery of Materials for Clean Energy in the Era of Smart Automation. *Nat. Rev. Mater.* **2018**, *3* (5), 5–20. https://doi.org/10.1038/s41578-018-0005-z.

(6) Armand, M.; Endres, F.; MacFarlane, D. R.; Ohno, H.; Scrosati, B. Ionic-Liquid Materials for the Electrochemical Challenges of the Future. *Nat. Mater.* **2009**, *8* (8), 621–629. https://doi.org/10.1038/nmat2448.

(7) Sheldon, R. A. Engineering a More Sustainable World through Catalysis and Green Chemistry. *J. R. Soc. Interface* **2016**, *13* (116), 20160087. https://doi.org/10.1098/rsif.2016.0087.

(8) Newsam, J. M.; Schüth, F. Combinatorial Approaches as a Component of High-Throughput Experimentation (HTE) in Catalysis Research. *Biotechnol. Bioeng.* **1999**, *61* (4), 203–216. https://doi.org/10.1002/(SICI)1097-0290(1998)61:4<203::AID-CC3>3.0.CO;2-V.

(9) Tom, G.; Schmid, S. P.; Baird, S. G.; Cao, Y.; Darvish, K.; Hao, H.; Lo, S.; Pablo-García, S.; Rajaonson, E. M.; Skreta, M.; Yoshikawa, N.; Corapi, S.; Akkoc, G. D.; Strieth-Kalthoff, F.; Seifrid, M.; Aspuru-Guzik, A. Self-Driving Laboratories for Chemistry and Materials Science. *Chem. Rev.* **2024**, *124* (16), 9633–9732. https://doi.org/10.1021/acs.chemrev.4c00055.

(10) Soldatov, M. A.; Butova, V. V.; Pashkov, D.; Butakova, M. A.; Medvedev, P. V.; Chernov, A. V.; Soldatov, A. V. Self-Driving Laboratories for Development of New Functional Materials and Optimizing Known Reactions. *Nanomaterials* **2021**, *11* (3), 619. https://doi.org/10.3390/nano11030619.